Composite Structures 92 (2010) 818–825

Contents lists available at ScienceDirect

Composite Structures

journal homepage: www.elsevier.com/locate/compstruct

Transverse shear stress distribution through thickness near an internal part-through elliptical hole in a stretched plate

Reaz A. Chaudhuri *

Department of Materials Science and Engineering, 122 S. Central Campus Dr., Room 304, University of Utah, Salt Lake City, UT 84112-0560, United States

ARTICLE INFO

Article history:
Available online 11 August 2009

Keywords:
Part-through hole
Internal or embedded elliptical cylindrical hole
Wedge singularity
Compatibility
Boundary layer effect
Transverse shear deformation

ABSTRACT

A semi-analytical post-processing method, termed the equilibrium/compatibility method here, is used for computation of hitherto unavailable through-thickness variation of transverse shear stresses in the vicinity of the circumferential re-entrant corner line of an internal part-through elliptical cylindrical hole weakening an edge-loaded rectangular plate. A C^0-type triangular "composite" plate element, based on the assumptions of transverse inextensibility and piece ("layer")-wise constant shear-angle theory (LCST), is employed to first compute the inplane stresses and "layer"-wise through-thickness average transverse shear stresses. These serve as the starting point for computation of through-thickness distribution of transverse shear stresses in the vicinity of the circumferential re-entrant corner line of the internal part-through elliptical hole. As in the case of its circular counterpart, the transverse shear stresses computed by the conventional equilibrium method (EM) are, in contrast, in serious error in the presence of the circumferential re-entrant corner line singularity arising out of the internal part-through elliptical hole, and are found to violate the compatibility condition. The computed maximum transverse shear stress can be high enough to cause catastrophic transverse shear fracture in the shape of a cone, of elliptical cross-section starting from the circumferential re-entrant corner line of the internal part-through hole. The results computed by the present analysis are in line with a three-dimensional asymptotic analysis.

1. Introduction

Embedded or internal part-through elliptical holes are more realistic representations of internal crack-like flaws and damages that invariably nucleate during the manufacturing process and propagate during service with catastrophic consequences [1–3]. The presence of internal part-through holes inside slabs or sheets is unavoidable in practice. A part of the internal material may be missing as a result of faulty manufacturing techniques.

Although the problems concerning the weakening effects of through-thickness circular or elliptical holes have a long history [4–8], the issues of stress concentration and stress singularity in the vicinity of internal part-through circular or elliptical holes have until recently remained a virgin territory [1–3]. The fact that these holes can cause severe cross-sectional warping resulting in transverse shear stresses even in a uniformly stretched plate, and as a result may initiate shear failure is a matter of serious concern to structural designers. Additionally, these transverse stresses in the neighborhood of such a hole in an edge-loaded homogeneous isotropic plate vary through the thickness, which brings out the three-dimensional effect even in a thin plate weakened by such a part-through hole [1–3]. Finally and most importantly, the effect of stress singularity in the neighborhood of the circumferential re-entrant corner line of the part-through internal or embedded hole weakening a plate is also of serious concerns because of its role in crack initiation [9].

Although reasonably accurate (finite element based) post-processing type methods for determination of interlaminar or transverse shear stresses in homogeneous and laminated plates and shells have been developed almost two decades earlier [10–18], a detailed review of the literature reveals that till recently the issue of determination of transverse shear stresses in the vicinity of an internal (or embedded) part-through hole weakening a plate subjected to all-round tension has remained unaddressed in the literature [19]. Majority of the finite element based post-processing approaches employ equilibrium equations of three-dimensional elasticity theory, referred to here as the equilibrium method, the only exceptions being Chaudhuri and Seide [12], and Chaudhuri [13]. These authors have introduced a semi-analytical post-processing method, termed the equilibrium/compatibility method, wherein both the equilibrium equations as well as interfacial compatibility conditions are satisfied in the point-wise sense. The latter approach has recently been employed for computation of hitherto

* Tel.: +1 801 581 6282; fax: +1 801 581 4816.
E-mail address: r.chaudhuri@utah.edu

0263-8223/$ - see front matter © 2009 Elsevier Ltd. All rights reserved.
doi:10.1016/j.compstruct.2009.08.019

The distribution of the components of displacement for the ith layer, based on the above assumptions, can be written as follows [25–27]:

$$u_m^{(i)}(z) = a_b^{(i)}(z)\bar{u}_m^{(i)} + a_t^{(i)}(z)\bar{u}_m^{(i+1)}, \quad m = \alpha, \beta, \tag{2a}$$

$$w^{(i)}(z) = w, \tag{2b}$$

where

$$a_b^{(i)}(z) = \left[H(Z-\bar{d}_i) - H(Z-\bar{d}_{i+1})\right]\left(1 - \frac{Z-\bar{d}_i}{t_i}\right), \tag{3a}$$

$$a_t^{(i)}(z) = \left[H(Z-\bar{d}_i) - H(Z-\bar{d}_{i+1})\right]\left(\frac{Z-\bar{d}_i}{t_i}\right), \tag{3b}$$

with

$$\bar{d}_i = \sum_{m=1}^{i-1} t_m, \quad \bar{d}_1 = 0, \quad \bar{d}_{N+1} = t. \tag{4}$$

$H(Z)$ is Heavyside or unit step function. α and β are general curvilinear coordinates in the plane of the plate. $Z = z + \bar{d}_i$ denotes transverse direction, and is measured from the bottom surface of the plate.

The quadratic shape functions used for the triangular element are best expressed in terms of area coordinates as shown below:

$$\{\phi\}^T = \{\zeta_1(2\zeta_1 - 1),\ 4\zeta_1\zeta_2,\ \zeta_2(2\zeta_2 - 1),\ 4\zeta_2\zeta_3,\ \zeta_3(2\zeta_3 - 1),\ 4\zeta_3\zeta_1\} \tag{5}$$

where ζ_k, $k = 1, 2, 3$ represents area coordinates. The assumed displacement potential energy based finite element equations are available elsewhere [1–3], and will not be repeated here in the interest of brevity of presentation. As a first step, the boundary of an elliptical hole is modeled using the straight-sided version of the present triangular element in question (see Fig. 2), which behaves more like a subparametric element, while its curvilinear counterpart would behave similar to an isoparametric element. In the case of a subparametric finite element, the error in strain energy due to domain approximation, $O(h^3)$, dominates its counterpart due to usual finite element approximation, $O(h^4)$, as suggested by Berger's lemma [31].

Once the nodal displacements are computed using the finite element method, the "layer"-element stresses can be obtained using the following relation [12]:

$$\{\sigma^{(i)}(z)\}^T = [C^{(i)}][A^{(i)}(z)]\left[B_j^{(i)}\right]\left\{d_j^{(i)}\right\}, \tag{6}$$

where

$$\{\sigma^{(i)}(z)\}^T = \left\{\sigma_x^{(i)}(z),\ \sigma_y^{(i)}(z),\ \tau_{xy}^{(i)}(z),\ \bar{\tau}_{xz}^{(i)},\ \bar{\tau}_{yz}^{(i)}\right\}, \tag{7}$$

in which $[A^{(i)}(z)]$, $\left[B_j^{(i)}\right]$, $\left\{d_j^{(i)}\right\}$ and $[C^{(i)}]$ are as given in Appendix.

3. Determination of transverse shear stresses using the equilibrium/compatibility method

The assumptions of "layer"-wise constant shear-angle theory (LCST) implies parabolic variation of transverse (interlaminar) shear stresses through the thickness of a "layer" by virtue of satisfying the first two equations of equilibrium. This implies, for example, that $\tau_{xz}^{(i)}(z)$ is of the form [12,13]:

$$\tau_{xz}^{(i)}(z) = N_1(z)\bar{f}_1^{(i)} + N_2(z)\bar{f}_2^{(i)} + N_3(z)\bar{f}_3^{(i)}, \tag{8}$$

where z is the transverse coordinate local to the ith layer, and is measured from its bottom surface. $\bar{f}_1^{(i)}$, $\bar{f}_2^{(i)}$ and $\bar{f}_3^{(i)}$ represent $\tau_{xz}^{(i)}(z)$ at the bottom, middle and top surface, respectively, of the ith layer. $N_1(z)$, $N_2(z)$ and $N_3(z)$ are one-dimensional quadratic shape functions, defined by [12,13]

$$N_1(z) = 1 - \frac{3z}{t_i} + \frac{2z^2}{t_i^2}, \quad N_2(z) = \frac{4z}{t_i} - \frac{4z^2}{t_i^2}, \quad N_3(z) = -\frac{z}{t_i} + \frac{2z^2}{t_i^2}. \tag{9}$$

τ_{xz} distribution through the thickness of an N-layer plate, therefore, requires $3N$ unknown parameters, which, in turn, ask for $3N$ equations. The present equilibrium/compatibility method supplies these equations, by (i) forcing τ_{xz} to vanish on the top and bottom surfaces of the plate (two equations), (ii) satisfying continuity of τ_{xz} at each "interface" ($N-1$ equations), (iii) identifying $\bar{\tau}_{xz}^{(i)}$, as computed by Eqs. (6) and (7) of Section 2 above, as the through-the-layer-thickness average of $\tau_{xz}^{(i)}(z)$ (N equations), and (iv) satisfying the compatibility condition by computing jump in $\tau_{xz,z}$ at each "interface" utilizing the first equation of equilibrium in terms of stresses, and equating it to zero ($N-1$ equations). A rigorous proof of the "interfacial" compatibility condition is given in Section 4 below.

The conditions (i) and (ii) above imply

$$\bar{f}_1^{(1)} = \bar{f}_3^{(N)} = 0, \tag{10}$$

$$\bar{f}_1^{(i)} = \bar{f}_3^{(i-1)}, \quad i = 2, \ldots, N. \tag{11}$$

The condition (iii) yields

$$\frac{1}{t_i}\int_0^{t_i} \tau_{xz}^{(i)}(z)dz = [0,\ 0,\ 0,\ 0,\ 0,\ 0,\ G,\ 0]\left[B_j^{(i)}\right]\left\{d_j^{(i)}\right\}, \quad \text{for } i = 1, \ldots, N. \tag{12}$$

Here $z = 0$ indicates the bottom of a layer.

Eq. (12) can, with the help of Eqs. (8)–(10), be written as follows:

$$\left(\frac{1}{6}\bar{f}_1^{(i)} + \frac{2}{3}\bar{f}_2^{(i+1)} + \frac{1}{6}\bar{f}_3^{(i+1)}\right) = [0,\ 0,\ 0,\ 0,\ 0,\ 0,\ G,\ 0]\left[B_j^{(i)}\right]\left\{d_j^{(i)}\right\}, \quad \text{for } i = 2, \ldots, N-1 \tag{13a}$$

$$\left(\frac{2}{3}\bar{f}_2^{(1)} + \frac{1}{6}\bar{f}_3^{(1)}\right) = [0,\ 0,\ 0,\ 0,\ 0,\ 0,\ G,\ 0]\left[B_j^{(1)}\right]\left\{d_j^{(1)}\right\}, \tag{13b}$$

$$\left(\frac{1}{6}\bar{f}_3^{(N-1)} + \frac{2}{3}\bar{f}_2^{(N)}\right) = [0,\ 0,\ 0,\ 0,\ 0,\ 0,\ G,\ 0]\left[B_j^{(N)}\right]\left\{d_j^{(N)}\right\}, \tag{13c}$$

The left and right sides of the remaining $N-1$ equations are given by the condition (iv) above, and are obtained by using Eqs. (8) and (9) and the first equation of equilibrium, respectively.

The compatibility condition in the form of vanishing jump in $\tau_{xz,z}$ at the $(i+1)$th interface is given by Eq. (19) as follows:

$$J_x^{(i+1)} = \frac{\partial \tau_{xz}^{(i+1)}(0)}{\partial z} - \frac{\partial \tau_{xz}^{(i)}(t_i)}{\partial z} = 0, \tag{14a}$$

which, with the help of Eq. (8), is given by

$$J_x^{(i+1)} = \left[\frac{\partial N_1(z)}{\partial z}\bar{f}_3^{(i)} + \frac{\partial N_2(z)}{\partial z}\bar{f}_2^{(i+1)} + \frac{\partial N_3(z)}{\partial z}\bar{f}_3^{(i+1)}\right]_{z=0} - \left[\frac{\partial N_1(z)}{\partial z}\bar{f}_3^{(i-1)} + \frac{\partial N_2(z)}{\partial z}\bar{f}_2^{(i)} + \frac{\partial N_3(z)}{\partial z}\bar{f}_3^{(i)}\right]_{z=t_i} = 0, \tag{14b}$$

which, with the help of Eq. (9), finally becomes

$$J_x^{(i+1)} = -\frac{1}{t_i}\bar{f}_3^{(i-1)} + \frac{4}{t_i}\bar{f}_2^{(i)} - 3\left(\frac{1}{t_i} + \frac{1}{t_{i+1}}\right)\bar{f}_3^{(i)} + \frac{4}{t_{i+1}}\bar{f}_2^{(i+1)} - \frac{1}{t_{i+1}}\bar{f}_3^{(i+1)} = 0, \quad \text{for } i = 2, \ldots, N-2, \tag{15a}$$

$$J_x^{(2)} = \frac{4}{t_1}\bar{f}_2^{(1)} - 3\left(\frac{1}{t_1} + \frac{1}{t_2}\right)\bar{f}_3^{(1)} + \frac{4}{t_2}\bar{f}_2^{(2)} - \frac{1}{t_2}\bar{f}_3^{(2)} = 0, \tag{15b}$$

$$J_x^{(N)} = -\frac{1}{t_{N-1}}\bar{f}_3^{(N-2)} + \frac{4}{t_{N-1}}\bar{f}_2^{(N-1)} - 3\left(\frac{1}{t_{N-1}} + \frac{1}{t_N}\right)\bar{f}_3^{(N-1)} - \frac{4}{t_N}\bar{f}_2^{(N)} = 0. \tag{15c}$$

Eqs. (10), (11), (13) and (15) determine the $3N$ unknown parameters required for describing the $\tau_{xz}(z)$ distribution through the thickness of the N-"layer" isotropic plate under investigation. Following an identical procedure and using the second equation of equilibrium, $\tau_{yz}(z)$ distribution through the plate thickness can be determined. $\tau_{nz}(z)$ and $\tau_{sz}(z)$ can be obtained by the usual coordinate transformation.

4. Proof of the "interfacial compatibility condition

The first equation of equilibrium is given by

$$\frac{\partial \tau_{xz}^{(i)}}{\partial z} = -\sigma_{xm,m}^{(i)}(z), \quad m = 1\ (=x),\ 2\ (=y), \tag{16}$$

in which a repeated index such as m implies summation. Integration over the surface area of the triangular element and application of the divergence theorem on the right side of the equation yields

$$\iint_{S_j} \frac{\partial \tau_{xz}^{(i)}}{\partial z} dS = -\iint_{S_j} \sigma_{xm,m}^{(i)}(z) dS = -\int_{\Gamma_j} \sigma_{xm}^{(i)}(z) n_m d\Gamma, \quad m = 1\ (=x),\ 2\ (=y) \tag{17}$$

Since for quadratic shape functions $\sigma_{xm,m}^{(i)}$ is constant with respect to x, y, integrating Eq. (16) over the area of the element and dividing by the same will not alter anything. This step yields

$$\frac{\partial \tau_{xz}^{(i)}}{\partial z} = -\frac{1}{S_j}\left[\int_{\Gamma_j} \sigma_{xm}^{(i)}(z) n_m d\Gamma_j\right] = -\frac{1}{S_j}\left[\sum_{k=1}^{3} \int_0^{l_j^{(k)}} \sigma_{xm}^{(i)}(z) n_m^{(k)} d\Gamma_j^{(k)}\right], \quad m = 1\ (=x),\ 2\ (=y). \tag{18}$$

Finally, following Chaudhuri and Seide [12], and Chaudhuri [13], the jump in $\frac{\partial \tau_{xz}(z)}{\partial z}$ at the $(i+1)$th "interface" can now be computed as follows:

$$J_x^{(i+1)} = \frac{\partial \tau_{xz}^{(i+1)}(0)}{\partial z} - \frac{\partial \tau_{xz}^{(i)}(t_i)}{\partial z} = -\frac{1}{S_j}\left[\sum_{k=1}^{3} \int_0^{l_j^{(k)}} [\sigma_{xm}^{(i+1)}(0) - \sigma_{xm}^{(i)}(t_i)] n_m^{(k)} d\Gamma_j^{(k)}\right] = 0, \quad \text{for } m = 1\ (=x),\ 2\ (=y), \text{ and } i = 1, \ldots, N-1. \tag{19}$$

Eq. (19) constitutes the required compatibility equation, when a weak or integral form of solution (in Sobolev space, H^1) is sought with convergence in the L_2 norm [19]. This equation is the counterpart of the compatibility (differential) equation (see the last of Eq. (4), p. 101, Fung [32]) when strong or differential form of solution is sought with convergence in the sup norm.

5. Location of exceptional points for the transverse shear stresses

The existence and location of special points, where the transverse shear stresses are exceptionally accurate, has been explained from a physical as well as rigorous mathematical point of view by Chaudhuri and Seide [12]. They have concluded that the centroid of the quadratic triangular element is the point of exceptional accuracy for the transverse shear stresses. Mathematically speaking, since the transverse shear stresses $\tau_{xz}(z)$ and $\tau_{yz}(z)$ use equilibrium equations in computing jumps at the "layer-interfaces" and hence involve the second derivatives of displacements with respect to x and y, these stresses are in error at a typical point by $O(h^{k-2})$ and on the average by $O(h^{k-1})$ for displacement functions $u^h \in S^h$ of degree $k-1$ (see Chaudhuri and Seide [12], and Strang and Fix [31] for the notation used here). These errors must alternate in sign, and there must exist exceptional points for the transverse shear stresses, which are the loci of centroids of the triangular element interfaces.

6. Numerical results and discussions: a rectangular isotropic plate weakened by an internal part-through elliptical cylindrical hole under all-round uniform tension

The plate is as shown in Fig. 1. A and A′ denote bottom and top corner points, the loci of which represent circumferential re-entrant corner lines of an internal part-through elliptical cylindrical hole weakening an edge-loaded rectangular plate in Fig. 1a. The following geometric parameters are selected:

$L = 50.8$ cm (20 in.), $b = 35.56$ cm (14 in.), $t = 0.762$ cm (0.3 in.), $a = 5.04$ cm (2 in.), $c = 2.54$ cm (1 in.), $h = 0.504$ cm (0.2 in.). Young's modulus, E, and Poison's ratio, ν, of steel are 206.85 GPa (30 Msi) and 0.3, respectively. The plate is subjected to all-round tension, $q = 689.5$ kPa (100 psi). It is discretized in the thickness direction into three fictitious layers, the middle one having the same thickness as that of the internal part-through elliptical hole.

Symmetry condition permits us to model a quarter of the plate in the x–y plane and half the thickness (Fig. 2). A mesh generator has been coded to generate a mesh of triangular elements in n, s elliptical coordinate system except those located in the neighborhood of four corner points of the quarter plate. Symmetry with respect to the middle surface along with the assumption of transverse inextensibility also produces vanishing transverse displacements at all the nodes. The inplane displacement symmetry conditions give rise to vanishing y-direction displacement along the x-axis (line AB) and vanishing x-direction displacement along the y-axis (line OCD) for the nodes lying on the bottom surface and the fictitious interface. For the nodes lying on the middle surface, the above symmetry conditions become vanishing y-direction displacement along the line AB and vanishing x-direction displacement along the line CD, with the elliptical boundary of the part-through hole remaining traction free. Uniform tension is applied along the lines BE and DE.

The finite element results presented in this section for computation of transverse shear stresses using the equilibrium method have been obtained first by using the quintic order of integration scheme (full integration), and later verified by using the quadratic order or reduced integration. The transverse shear stresses computed by the present equilibrium/compatibility method, have been obtained by using the reduced integration scheme only.

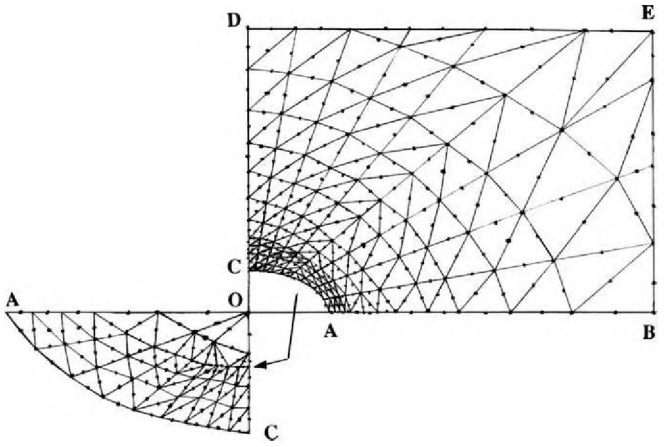

Fig. 2. Finite element model for a rectangular plate weakened by an internal part-through elliptical hole.

The presence of the part-through hole, even in a thin homogeneous isotropic plate, causes severe cross-sectional warping that usually characterizes the bending of thick plates and laminates with large variation of fiber orientation in consecutive layers. The cross-sectional warping dies down at a distance away from the boundary of the part-through hole [1,3].

Fig. 3 displays the transverse shear stress, $\tau_{nz}^{(1)}(t_1) = \tau_{nz}^{(2)}(0)$, computed near the re-entrant corner line around the circumference of the internal part-through elliptical cylindrical hole computed using the present equilibrium/compatibility method, and its comparison with that computed using the conventional equilibrium method [10]. These values are computed at the centroids of the triangular elements adjacent to the part-through hole boundary (see also Table 1). Table 1 and Fig. 3 show that barring the initial trough-like feature between $s = 15°$ and 45° and some minor oscillations, $\tau_{nz}^{(1)}(t_1) = \tau_{nz}^{(2)}(0)$ at the circumference of the part-through elliptical cylindrical hole appears to remain constant with s from $s = 0$ to $\pi/2$, in a manner reminiscent of its circular counterpart [19]. The trough-like feature in the $\tau_{nz}^{(1)}(t_1) = \tau_{nz}^{(2)}(0)$ vs. s curves can be attributed to the stronger influence of the boundary $y = b/2$ compared to that of the edge $x = L/2$ on the distribution of $\tau_{nz}^{(1)}(t_1) = \tau_{nz}^{(2)}(0)$ around the circumferential re-entrant corner line of the embedded elliptical cylindrical hole. $\tau_{sz}^{(1)}(t_1) = \tau_{sz}^{(2)}(0)$ values computed at the centroids of the same elements are found to be negligible (see Table 1), since $\tau_{sz}(z)$ is non-singular at the circumferential re-entrant corner line of the internal part-through elliptical hole [9].

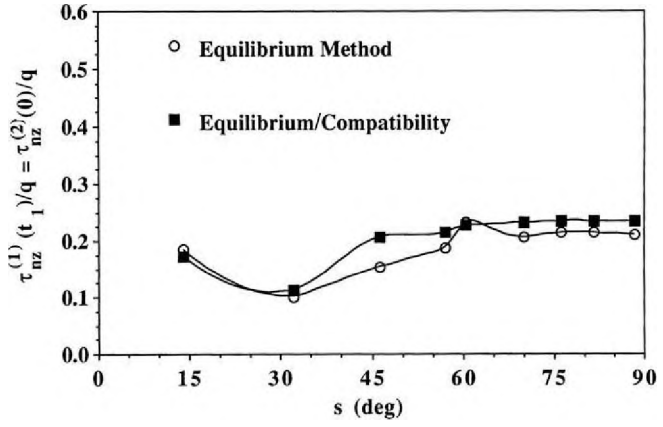

Fig. 3. Variation of the normalized transverse shear stress, τ_{nz}, around the circumference of an internal part-through elliptical cylindrical hole (see Table 1 for location of points).

Table 1
Variation of transverse shear stresses around the circumference of an internal part-through elliptical cylindrical hole.

Location		s (°)	Equilibrium method		Equilibrium/compatibility method	
x (in.)	y (in.)		$\tau_{nz}(t_1)/q$	$\tau_{sz}(t_1)/q$	$\tau_{nz}(t_1)/q$	$\tau_{sz}(t_1)/q$
2.045	0.127	13.980	0.185	−0.03	0.173	−0.003
1.573	0.309	32.050	0.101	0.09	0.113	0.02
1.839	0.481	46.294	0.153	0.001	0.207	0.03
1.650	0.638	57.120	0.187	0.01	0.215	0.02
1.501	0.727	60.422	0.232	0.06	0.227	0.04
1.233	0.850	70.070	0.206	0.02	0.232	0.02
0.928	0.948	76.253	0.214	0.02	0.235	0.02
0.595	1.017	81.688	0.214	0.02	0.235	0.01
0.116	1.062	88.438	0.210	0.02	0.234	0

Fig. 4 exhibits variation of $\tau_{nz}(z)$ at $x = 5.194$ cm (2.045 in.), $y = 0.323$ cm (0.127 in.), computed using the conventional equilibrium method as well as by the present method. As can be seen from Fig. 4, the transverse shear stress distribution through the thickness predicted by the equilibrium method is in serious error. Since the material is homogeneous, τ_{nz} vs. z curve cannot have a "corner", because that would imply jumps (or discontinuities) in the stresses, $\sigma_n(z)$ and $\tau_{ns}(z)$, which, in turn, would imply jumps in strains, $\varepsilon_n(z)$ and $\gamma_{ns}(z)$, and consequently discontinuities in in-plane displacements at that particular z, i.e., the compatibility equations are violated. The apparent reason behind this lack of accuracy in the result computed by the equilibrium method is that there is only one integration constant. Needless to say, this cannot make the computed transverse shear stress vanish on both the bottom and top surfaces of plate, unless symmetry with respect to the middle surface is invoked [19]. The error in $\frac{\partial \sigma_x(z)}{\partial x} + \frac{\partial \tau_{xy}(z)}{\partial y}$ computed by the finite element method is "body force" like (constant through thickness in uniform stretching problems), and is of the order of $\frac{\partial \tau_{xz}(z)}{\partial z}$. When $\tau_{xz}(z)$ is computed by the equilibrium method by integrating the first equation of equilibrium through thickness, this error shows up as a straight line. In the case of a symmetrically (with respect to the middle surface) placed internal part-through elliptical hole weakening a homogeneous isotropic plate subjected to uniform stretching, if $\tau_{xz}(z)$ through half the thickness is computed by using the equilibrium method, and the same through the other half is obtained by using symmetry, this would result in the formation of a "corner" in the curve at the mid-surface. This "corner" cannot be acceptable because of the violation of the compatibility condition at the mid-surface of the plate in the immediate neighborhood of the circumferential re-entrant corner line.

It is worthwhile to note from Fig. 5 of Chaudhuri [3] that σ_x at the fictitious "interface" (circumferential re-entrant corner line) experiences a jump at the circumference of the internal part-through elliptical hole, and that the maximum stress occurs at this corner. The slope of the above curve (i.e., $\sigma_{x,x}$) at the circumferential corner is approximately $\tan(\pi/2) = \infty$, which, when substituted into the equilibrium equations, will yield singular transverse stresses τ_{xz} and σ_z in that neighborhood. Fig. 5 displays the state of stress in a 270° wedge shaped plane section normal to the circumferential line of intersection of the boundary wall of the internal part-through elliptical hole with its ceiling or floor (locus of point A or A′ in Fig. 1). The local coordinate system is, as shown in Fig. 5, comprised of R, which denotes the radial direction from a point located on the circumferential line of intersection of the bottom interior surface of the plate and the hole, ϕ, which denotes the angular direction measured counterclockwise from the hole surface, and s,

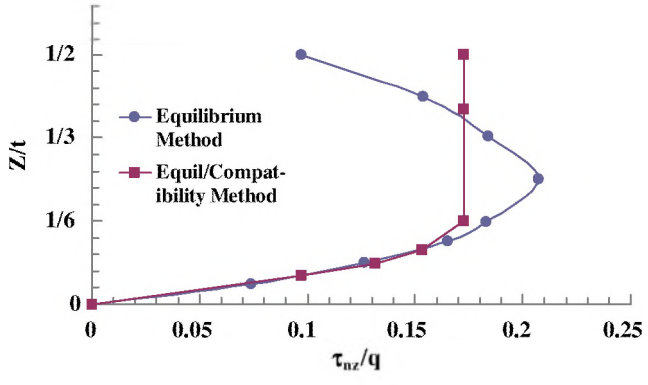

Fig. 4. Through-thickness variation of normalized transverse shear stress, τ_{nz}/q, in the vicinity of an internal part-through elliptical cylindrical hole ($x = 5.194$ cm (2.045 in.), $y = 0.323$ cm (0.127 in.)).

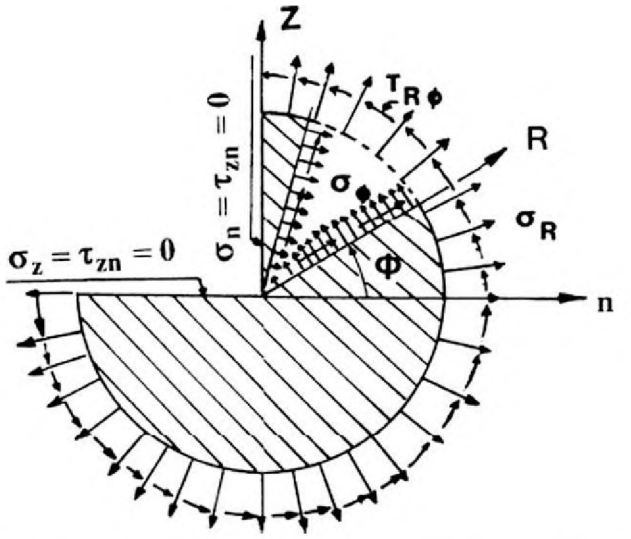

Fig. 5. Stresses on a plane 270°-wedge radial section of a plate in the neighborhood of an internal part-through elliptical cylindrical hole.

which is positive counterclockwise (looking from top) along the circumferential line of intersection of the interior surface of the plate and the hole surface. The stresses, σ_R, σ_φ, $\tau_{R\varphi}$ and σ_s are singular in the vicinity of the circumferential re-entrant corner line of the internal part-through hole [9]. This translates into rendering σ_n, τ_{nz}, σ_z and σ_s singular in that neighborhood.

Strength of the singularity for a plane wedge was first discussed by Williams [33]. However, in the present case, where the state of stress is three-dimensional and the wedge front is elliptically curved, no asymptotic solution is currently available. Chaudhuri [9] has recently derived the strength of the stress singularity in the neighborhood of the circumferential re-entrant corner line (i.e., the line of intersection of an embedded circular cylindrical part-through hole and an interior z-plane of an isotropic plate), subjected to far-field extension–bending (mode I), inplane shear-twisting (mode II), and torsional (mode III) loadings. The stress field varies as $R^{-(0.456)}$ in the vicinity of the circumferential corner line of the part-through hole which is identical to the plane strain version of Williams' [33] solution. It is well known that the strength of this stress singularity does not depend on the geometrical shape of the curve. In the presence of a stress singularity of this kind, the stress gradients are also significantly large, which combined with the constant (through the thickness) term causes the above-mentioned "body force' like error upon integration with respect to z, when the equilibrium method is used. This implies that the artificial "corner" (see Fig. 4) will appear whenever inplane stress gradients do not vanish at the mid-surface of the plate, and consequently the equilibrium method will fail to deliver accurate results for the transverse shear stresses.

The above-mentioned "corner" and the associated "body force" like error can be eliminated by using the present method as can be seen from Fig. 4, because of its satisfaction of "interface" compatibility condition, given by Eq. (19), in the form of the condition (iv) of Section 3, which is the vanishing of the "interfacial" discontinuity, given by Eq. (14) or Eq. (19).

7. Summary and conclusions

A semi-analytical method, termed the equilibrium/compatibility method here, is used for computation of hitherto unavailable through-thickness variation of transverse shear stresses in the vicinity of the circumferential re-entrant corner line of an internal part-through elliptical cylindrical hole weakening an edge-loaded rectangular plate. A C^0-type triangular "composite" plate element, based on the assumptions of transverse inextensibility and piece ("layer")-wise constant shear-angle theory (LCST), is employed to first compute the inplane stresses and "layer"-wise through-thickness average transverse shear stresses, which serve as the starting point for computation of through-thickness distribution of transverse shear stresses in the vicinity of the circumferential re-entrant corner line of the internal part-through elliptical cylindrical hole. The present investigation confirms the conclusion reached earlier in the case of its circular counterpart [19] in regards to the accuracy (or lack of it) of the stresses computed using the conventional (assumed displacement potential energy based) finite element analysis and computed FEM-based post-processing analysis results for transverse shear stresses in the vicinity of a stress singularity, such as the circumferential corner line of an internal elliptical cylindrical hole. Eq. (19) constitutes the required compatibility equation, when a weak or integral form of solution (in Sobolev space, H^1) is sought with convergence in the L_2 norm [19]. This equation is the counterpart of the compatibility (differential) equation when strong or differential form of solution is sought with convergence in the sup norm. This problem is not restricted to the FEM alone, but pervades all over discrete integral equations based methods, such as the FFT (Fast Fourier Transform) or BIE (Boundary Integral Equations). The following important conclusions are drawn from the numerical results of the present finite element based post-processing analysis:

(i) The transverse shear stress, τ_{nz}, computed using the conventional equilibrium method is in serious error in the presence of the stress singularity at the circumferential re-entrant corner line of an internal part-through elliptical cylindrical hole. This is because τ_{nz} is singular [9]. This error is "body force" like, and is due to the violation of the compatibility equation in the presence of stress singularity.

(ii) The above error can be eliminated by using the present method because of its satisfaction of "interface" compatibility condition in the vicinity of the circumferential re-entrant corner line singularity arising out of the internal part-through elliptical hole.

(iii) barring the initial trough-like feature between $s = 15°$ and 45° and some minor oscillations, $\tau^{(1)}_{nz}(t_1) = \tau^{(2)}_{nz}(0)$ at the circumference of the part-through elliptical cylindrical hole appears to remain constant with s from $s = 0$ to $\pi/2$, in a manner reminiscent of its circular counterpart.

(iv) The trough-like feature in the $\tau^{(1)}_{nz}(t_1) = \tau^{(2)}_{nz}(0)$ vs. s curves can be attributed to the stronger influence of the boundary $y = b/2$ compared to that of the edge $x = L/2$ on the distribution of $\tau^{(1)}_{nz}(t_1) = \tau^{(2)}_{nz}(0)$ around the circumferential re-entrant corner line of the embedded elliptical cylindrical hole.

(v) $\tau^{(1)}_{sz}(t_1) = \tau^{(2)}_{sz}(0)$ values computed in the vicinity of the circumferential re-entrant corner line of the embedded elliptical cylindrical hole are found to be negligible, since $\tau_{sz}(z)$ is non-singular at the circumferential re-entrant corner line of the internal part-through elliptical hole [9].

(vi) The computed transverse shear stress, τ_{nz}, can be as high as 17.3% (23% in the special case of a circular internal hole) of the applied far-field tensile stress and possibly higher (because it is singular), which can cause catastrophic shear fracture in the shape of a cone of elliptical cross-section emanating from the circumferential re-entrant corner line of the internal part-through hole. The results computed by the present analysis are in line with a three-dimensional asymptotic analysis [9].

The present analysis is currently being extended to the case of an internal elliptical hole weakening a cylindrical panel [34], and will be reported in a future paper.

Appendix A. Definitions of some matrices and vectors

$[A^{(i)}]$, $i = 1, \ldots, N$, referred to in Eq. (6), is given by

$$[A^{(i)}] = \begin{bmatrix} [A_b^{(i)}] & [A_t^{(i)}] & [0] \\ [0] & [0] & [A_s^{(i)}] \end{bmatrix}, \tag{A1}$$

where

$$[A_b^{(i)}] = \begin{bmatrix} 1-\frac{z}{t_i} & 0 & 0 \\ 0 & 1-\frac{z}{t_i} & 0 \\ 0 & 0 & 1-\frac{z}{t_i} \end{bmatrix}, \tag{A2a}$$

$$[A_t^{(i)}] = \begin{bmatrix} \frac{z}{t_i} & 0 & 0 \\ 0 & \frac{z}{t_i} & 0 \\ 0 & 0 & \frac{z}{t_i} \end{bmatrix}, \tag{A2b}$$

and

$$[A_s^{(i)}] = \begin{bmatrix} 1 & 0 \\ 0 & 1 \end{bmatrix}. \tag{A2c}$$

$\{d_j^{(i)}\}$, as referred to in Eq. (6), is given as follows:

$$\{d_j^{(i)}\}^T = \{\bar{u}_1^{(i)}, \bar{v}_1^{(i)}, \ldots, \bar{u}_6^{(i)}, \bar{v}_6^{(i)}, \bar{u}_1^{(i+1)}, \bar{v}_1^{(i+1)}, \ldots, \bar{u}_6^{(i+1)}, \bar{v}_6^{(i+1)}, \times w_1, \ldots, w_6\}. \tag{A3}$$

$[B_j^{(i)}]$, as referred to in Eq. (6), is given by

$$[B_j^{(i)}] = \begin{bmatrix} [R] & [0] & [0] \\ [0] & [R] & [0] \\ [M^{(i)}] & [N^{(i)}] & [T] \end{bmatrix}, \tag{A4}$$

whose submatrices are given as follows:

$$[R] = [[R_1] \cdots [R_k] \cdots [R_6]], \quad k = 1, \ldots, 6, \tag{A5a}$$

with

$$[R_k] = \begin{bmatrix} \phi_{k.1} & 0 \\ 0 & \phi_{k.2} \\ \phi_{k.2} & \phi_{k.1} \end{bmatrix}, \tag{A5b}$$

$$[T] = [[T_1] \cdots [T_k] \cdots [T_6]], \quad k = 1, \ldots, 6, \tag{A6a}$$

$$[T_k] = \begin{bmatrix} \phi_{k.1} & \\ & \phi_{k.2} \end{bmatrix}, \tag{A6b}$$

$$[N^{(i)}] = \left[\left[N_1^{(i)}\right] \cdots \left[N_k^{(i)}\right] \cdots \left[N_6^{(i)}\right]\right], \quad k = 1, \ldots, 6; \ i = 1, \ldots, N, \tag{A7a}$$

with

$$\left[N_k^{(i)}\right] = \begin{bmatrix} \frac{\phi_k}{t_i} & \\ & \frac{\phi_k}{t_i} \end{bmatrix}, \tag{A7b}$$

while

$$[M^{(i)}] = -[N^{(i)}], \quad i = 1, \ldots, N. \tag{A8}$$

ϕ_k, $k = 1, \ldots, 6$, referred to above in Eqs. (A5)–(A7), represent the shape function for the kth node of a triangular element interface, and is given by Eq. (5).

$[C^{(i)}]$, $i = 1, \ldots, N$, referred to in Eq. (6), can be written as follows:

$$[C^{(i)}] = \begin{bmatrix} \frac{E}{(1-\nu^2)} & \frac{\nu E}{(1-\nu^2)} & 0 & 0 & 0 \\ \frac{\nu E}{(1-\nu^2)} & \frac{E}{(1-\nu^2)} & 0 & 0 & 0 \\ 0 & 0 & G & 0 & 0 \\ 0 & 0 & 0 & G & 0 \\ 0 & 0 & 0 & 0 & G \end{bmatrix}. \tag{A9}$$

References

[1] Chaudhuri RA, Seide P. Triangular element for analysis of a stretched plate weakened by a part-through hole. Comput Struct 1986;24:97–105.
[2] Chaudhuri RA. Stress concentration around a part-through hole weakening a laminated plate. Comput Struct 1987;25:601–9.
[3] Chaudhuri RA. Weakening effects of internal part-through elliptic holes on homogeneous and laminated composite plates. Compos Struct 2007;81:362–73.
[4] Lekhnitskii SG. Stresses in infinite anisotropic plate weakened by elliptical hole. DAN SSR 1936:4.
[5] Green AE. Stress systems in isotropic and aeolotropic plates. V. Proc Roy Soc Lond Series A, Math Phys Sci 1945;184:231–52.
[6] Savin GN. Stress distribution around holes. Kiev: Naukova Dumka Press; 1968. Also, NASA TT F-601, 1970.
[7] Chaudhuri RA, Seide P. Triangular element for analysis of perforated plates under inplane and transverse loads. Comput Struct 1986;24:87–95.
[8] Chaudhuri RA. An eigenfunction expansion solution for three-dimensional stress field in the vicinity of the circumferential line of intersection of a bimaterial interface and a hole. Int J Fract 2004;129:361–84.
[9] Chaudhuri RA. Three-dimensional asymptotic stress field in the vicinity of the line of intersection of a circular cylindrical through/part-through open/rigidly plugged hole and a plate. Int J Fract 2003;122:65–88.
[10] Chaudhuri RA. An equilibrium method for prediction of transverse shear stresses in a thick laminated plate. Comput Struct 1986;23:139–46.
[11] Chaudhuri RA, Seide P. An approximate method for prediction of transverse shear stresses in a laminated shell. Int J Solids Struct 1987;23:1145–61.
[12] Chaudhuri RA, Seide P. An approximate semi-analytical method for prediction of interlaminar shear stresses in an arbitrarily laminated thick plate. Comput Struct 1987;25:627–36.
[13] Chaudhuri RA. A semi-analytical approach for prediction of interlaminar shear stresses in laminated general shells. Int J Solids Struct 1990;26:499–510.
[14] Engblom JJ, Ochoa OO. Finite element formulation including interlaminar stress calculations. Comput Struct 1986;23:231–49.
[15] Byun C, Kapania RK. Prediction of interlaminar stresses in laminated plates using global orthogonal interpolation polynomials. AIAA J 1992;30:2740–9.
[16] Noor AK, Kim YH, Peters JM. Transverse shear stresses and their sensitivity coefficients in multilayered composite panels. AIAA J 1994;32:1259–68.
[17] Rohwer K, Rolfes R. Calculating 3D stresses in layered composite plates and shells. Mech Compos Mater 1998;34:355–62.
[18] Chaudhuri RA, Balaraman K, Kunukkasseril VX. Admissible boundary conditions and solutions to internally pressurized thin arbitrarily laminated cylindrical shell boundary-value problems. Compos Struct 2008;86:385–400.
[19] Chaudhuri RA. Computation of transverse shear stresses in the vicinity of the circumferential re-entrant corner line of an internal part-through hole weakening an edge-loaded plate. Compos Struct 2009;89:315–20.
[20] Pipes RB, Pagano NJ. Interlaminar stresses in composite laminates under uniform axial extension. J Compos Mater 1970;4:538–48.
[21] Chaudhuri RA, Xie M. Free-edge stress singularity in a bimaterial laminate. Compos Struct 1998;40:129–36.
[22] Chaudhuri RA, Xie M. A tale of two saints: St. Venant and "St. Nick" — does St. Venant's principle apply to bi-material straight edge and wedge singularity problems? Compos Sci Technol 2000;60:2503–15.
[23] Chaudhuri RA, Chiu SJ. Three-dimensional asymptotic stress field at the front of an unsymmetric bimaterial wedge associated with matrix cracking or fiber break. Compos Struct 2007;78:254–63.
[24] Chaudhuri RA, Chiu SJ. Three-dimensional asymptotic stress field in the vicinity of an adhesively bonded scarf joint interface. Compos Struct 2009;89:475–83.
[25] Chaudhuri RA, Seide P. Triangular finite element for analysis of thick laminated plates. Int J Numer Methods Eng 1987;24:1203–24.
[26] Chaudhuri RA. Analysis of laminated shear-flexible angle-ply plates. Compos Struct 2005;67:71–84.
[27] Seide P, Chaudhuri RA. Triangular finite element for analysis of thick laminated shells. Int J Numer Methods Eng 1987;24:1563–79.
[28] Chaudhuri RA. A simple and efficient plate bending element. Comput Struct 1987;25:817–24.
[29] Chaudhuri RA. A degenerate triangular shell element with constant cross-sectional warping. Comput Struct 1988;28:315–25.

[30] Arfken G. Mathematical methods for physicists. 2nd ed.. New York: Academic Press; 1970.
[31] Strang G, Fix G. The finite element method. 3rd ed. Englewood Cliffs (NJ): Prentice-Hall; 1973.
[32] Fung YC. Foundations of solid mechanics. Englewood Cliffs (NJ): Prentice-Hall; 1965.
[33] Williams ML. Stress singularities resulting from various boundary conditions in angular corners of plates in extension. ASME J Appl Mech 1952;19:526–8.
[34] Chaudhuri RA. A new three-dimensional shell theory in general (non-lines-of-curvature) coordinates for analysis of curved paneis weakened by through/part-through holes. Compos Struct 2009;89:321–32.